



ELSEVIER

Contents lists available at ScienceDirect

Journal of Sound and Vibration

journal homepage: www.elsevier.com/locate/jsvi

Non-stationary random vibration analysis of a 3D train–bridge system using the probability density evolution method



Zhi-wu Yu, Jian-feng Mao*, Feng-qi Guo, Wei Guo

National Engineering Laboratory for High Speed Railway Construction & School of Civil Engineering, Central South University, Changsha 410075, China

ARTICLE INFO

Article history:

Received 29 September 2014

Received in revised form

30 October 2015

Accepted 4 December 2015

Handling Editor: J. Macdonald

Available online 22 December 2015

ABSTRACT

Rail irregularity is one of the main sources causing train–bridge random vibration. A new random vibration theory for the coupled train–bridge systems is proposed in this paper. First, number theory method (NTM) with $2N$ -dimensional vectors for the stochastic harmonic function (SHF) of rail irregularity power spectrum density was adopted to determine the representative points of spatial frequencies and phases to generate the random rail irregularity samples, and the non-stationary rail irregularity samples were modulated with the slowly varying function. Second, the probability density evolution method (PDEM) was employed to calculate the random dynamic vibration of the three-dimensional (3D) train–bridge system by a program compiled on the MATLAB[®] software platform. Eventually, the *Newmark- β* integration method and double edge difference method of total variation diminishing (TVD) format were adopted to obtain the mean value curve, the standard deviation curve and the time–history probability density information of responses. A case study was presented in which the ICE-3 train travels on a three-span simply-supported high-speed railway bridge with excitation of random rail irregularity. The results showed that compared to the Monte Carlo simulation, the PDEM has higher computational efficiency for the same accuracy, i.e., an improvement by 1–2 orders of magnitude. Additionally, the influences of rail irregularity and train speed on the random vibration of the coupled train–bridge system were discussed.

© 2015 Elsevier Ltd. All rights reserved.

1. Introduction

The dynamic problems of the coupled train–bridge system in a high-speed railway are challenging. The random vibration of the coupled train–bridge system is generally characterized by random dynamic excitations (e.g. earthquakes, wind load, and rail irregularity, etc.), and random system parameters (e.g. train parameters, and structural parameters, etc.). Rail irregularity is one of the primary sources causing the random vibration of train–bridge systems. However, the vibration theory for a train–bridge system with random excitation and random structural parameters has not been systematically built yet. To this end, the primary objective of this study is to investigate the random vibration caused by random rail irregularity.

* Correspondence to: National Engineering Laboratory for High Speed Railway Construction, Central South University, No. 22, Shaoshan Road, Changsha 410075, China.

E-mail address: csumjf@mail.csu.edu.cn (J.-f. Mao).

For decades, extensive studies have been conducted in the field of the coupled train–bridge vibration for high-speed railways. However, those studies have focused on the vibration excited by deterministic rail irregularity in the train–bridge system [1–5]. It is well known that a limited number of rail irregularity samples acting on the train–bridge system, either measured or artificially generated, is insufficient for characterizing the random train–bridge responses. Thus, it remains an urgent need to further study the train–bridge systems using the random vibration theory.

The random dynamic analysis of coupled train–bridge systems has been long studied. In 1976, Fryba [6] first investigated bridge random vibration caused by moving vehicles. Subsequently, researchers (e.g. Iwankiewicz [7], Sniady [8], Chu [9] and Zibdeh [10]) in the field of random vibration of train–bridge systems commonly employed in their simulation work the model of a load moving across the bridge, among which few considered the effect of rail irregularity. In fact, the random rail irregularity should be considered in the calculation due to its importance in the coupled train–bridge system. To date, several methods have been developed and applied for analyzing the random vibration of train–bridge systems (e.g. Monte Carlo Method (MCM), Pseudo Excitation Method (PEM) [11], etc.). The MCM has been adopted to generate samples for random track irregularities. Zeng [12] calculated the random response of a train–bridge system with hunting waves of the bogie frame measured or generated with MCM. Zhai [13–15] and Xia [16–18] made significant contributions in the field of coupled train–track–bridge system vibration, mainly with the method of MCM. Kardas-Cinal [19] obtained the spectral distribution of the derailment coefficient using a nonlinear model of the railway vehicle–track system excited by random rail irregularity. Lin [11,20] established the PEM for analyzing the random vibration of the coupled train–bridge system. With virtual inputs, PEM could efficiently obtain the response power spectrum and the standard deviation on the basis of the rail irregularity power spectrum. However, PEM cannot obtain the mean value of responses, and is therefore inadequate for application in train–bridge systems. Thus, MCM is the only method generally applicable in probabilistic mechanics, but the expensive computational costs required for sufficient accuracy also limits its use in engineering applications. Yet, it is still commonly used to provide reference solutions for comparison with those obtained by more efficient methods tailored to specific problems.

Li and Chen developed a generalized probability density evolution method (PDEM) [21–23], which contributed to the solution of the linear and nonlinear random vibration analyses of a system with random inputs. Based on the fundamental concepts of a random system, this method, as compared to MCM, could significantly improve the calculation efficiency, and is able to solve the random vibration problems involving random excitations and stochastic structural parameters as well. Inspired by this methodological framework, Yu and Mao [24] employed PDEM to analyze the vertical random vibration of the coupled train–bridge system with random train parameters and rail irregularity, and drew some insightful conclusions.

The primary objective of this study was to establish a stochastic harmonic function of rail irregularity [25] from the rail irregularity power spectrum density (PSD) by combining PDEM and number theoretical method (NTM). It was then used to select representative points of spatial frequencies and phases [22,26] for calculating random vibration of the train–bridge system. The calculation results including mean value curves, standard deviation curves and time-dependent probability density information were obtained. Examples and applications were presented and discussed as well.

2. Train–bridge random dynamic equation and probability density evolution method

2.1. Random dynamic equation of the train–bridge system

2.1.1. 3D train–bridge model

For the vehicle model, the following assumptions were made:

- (1) A train runs over the bridge at a constant speed.
- (2) Each car consists of one body, two bogies, and four wheel sets, which are modeled as rigid bodies. The primary and secondary suspension systems are modeled using linear springs and dampers.
- (3) The degrees of freedom (dofs) of the car bodies and bogies are y, θ, ψ, z , and φ , and the dofs of the wheel sets are y, θ , and z .
- (4) There are no sliding, climbing or derailment phenomena when the train is running on the rail, i.e., the wheels keep in contact with the rail surface.

A dynamic interaction model of the 3D train–bridge system [20] with random rail irregularity as the excitation is shown in Fig. 1, where an absolute coordinate system is adopted for the train–bridge system.

2.1.2. Equation for vehicle model

To highlight the random nature of rail irregularity as the load, first let ξ_q ($q = 1, 2, \dots, n_{pt}$) be a random variable of rail irregularity belonging to a random variable vector set Θ that contains random spatial frequencies $\tilde{\Omega}$ and phases $\tilde{\phi}$ discussed in the next section. Specifically, ξ_q can be expressed as $\xi_q = (\tilde{\Omega}_{q,1}, \tilde{\Omega}_{q,2}, \dots, \tilde{\Omega}_{q,N}, \tilde{\phi}_{q,1}, \tilde{\phi}_{q,2}, \dots, \tilde{\phi}_{q,N}) \in \Theta$, where n_{pt} is the total number of representative samples, and N is the number of spatial frequencies and phases.

Without loss of generality, by referring to Refs. [20,27], the vehicle motion can be established using the Lagrange's equations. With the assumptions discussed in Section 2.1 taken into account, the linearized dynamic equation of the vehicle

system is expressed as

$$\mathbf{M}_V \ddot{\mathbf{X}}_V + \mathbf{C}_V \dot{\mathbf{X}}_V + \mathbf{K}_V \mathbf{X}_V = \mathbf{F}_V(\xi_q, t) \tag{1}$$

where the subscript V denotes the vehicle, and $\mathbf{F}_V(\xi_q, t)$ denotes the random rail irregularity generated by rail irregularity power spectrum density with stochastic harmonic function (SHF) [25].

In fact, the dynamic equation of Eq. (1) contains nonlinear items and second-order items, e.g. the spring stiffness of suspension system. However, these items are linearized or neglected in this study.

The mass matrix in Eq. (1) is expressed as $\mathbf{M}_V = \text{diag}[\mathbf{M}_{V1}, \mathbf{M}_{V2}, \dots, \mathbf{M}_{Vi}, \dots, \mathbf{M}_{Vn}]$. The submatrices \mathbf{C}_{Vi} and \mathbf{K}_{Vi} have the same form in the damping matrix \mathbf{C}_V and the stiffness matrix \mathbf{K}_V . The random external force impulse $\mathbf{F}_V(\xi_q, t)$ is expressed as $\mathbf{F}_V = \text{column}[\mathbf{F}_{V1}, \mathbf{F}_{V2}, \dots, \mathbf{F}_{Vi}, \dots, \mathbf{F}_{Vn}]$. The response matrix \mathbf{X}_V is expressed as $\mathbf{X}_V = \text{column}[\mathbf{X}_{V1}, \mathbf{X}_{V2}, \dots, \mathbf{X}_{Vi}, \dots, \mathbf{X}_{Vn}]$. The

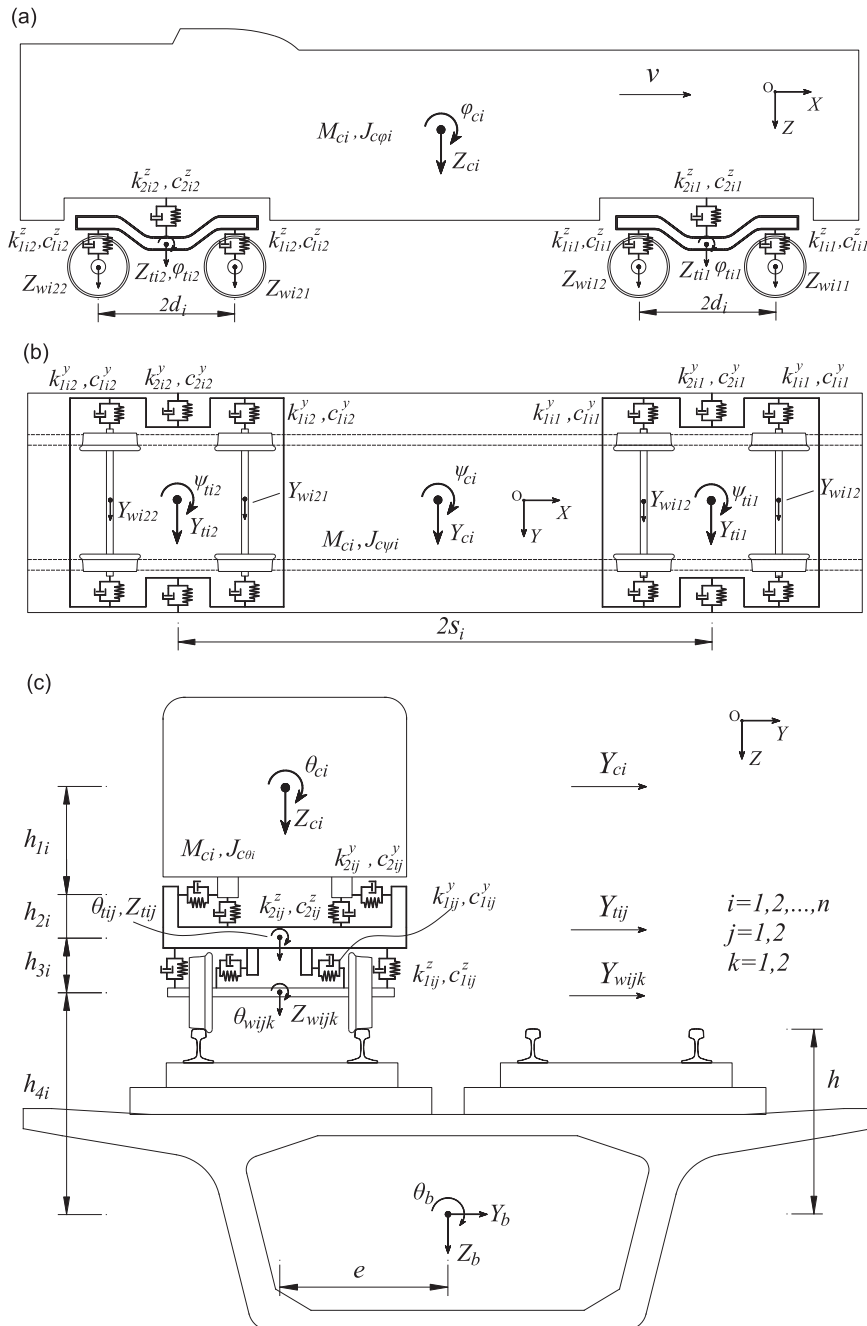


Fig. 1. Dynamic interaction model of the 3D train-bridge system: (a) lateral view; (b) top view; and (c) front view.

subscript n denotes the total number of the vehicular cars. The dynamic equation of i th car is expressed as:

$$\mathbf{M}_{Vi}\ddot{\mathbf{X}}_{Vi} + \mathbf{C}_{Vi}\dot{\mathbf{X}}_{Vi} + \mathbf{K}_{Vi}\mathbf{X}_{Vi} = \mathbf{F}_{Vi}(\xi_q, t) \tag{2}$$

where $i=1,2,\dots,n$.

The wheels of the vehicle are assumed to always remain in perfect contact with the rail surface, according to the wheel-rail relationship expressed on Section 2.1.4, hence the degrees of freedom of the wheel sets are not directly mentioned in Eq. (2). Thus, each car in Eq. (2) has 15 independent degrees of freedom (dof), and each car consists of one car-body and two bogies that are denoted by the subscripts c, t_1 and t_2 respectively. The response vectors are expressed as follows:

$$\mathbf{X}_{Vi} = [\mathbf{X}_{ci} \quad \mathbf{X}_{t_1i} \quad \mathbf{X}_{t_2i}]^T \tag{3a}$$

$$\mathbf{X}_{ci} = [Y_{ci} \quad \theta_{ci} \quad \psi_{ci} \quad Z_{ci} \quad \varphi_{ci}]^T \tag{3b}$$

$$\mathbf{X}_{t_ji} = [Y_{t_ji} \quad \theta_{t_ji} \quad \psi_{t_ji} \quad Z_{t_ji} \quad \varphi_{t_ji}]^T, j = 1, 2 \tag{3c}$$

Random rail irregularity is considered to be the random factor in Eq. (1). Referring to Ref. [20] and the definition expressed in Section 2.1.1, as well as to the wheel-rail geometrical relationship in Eq. (9), the stochastic mechanical impulse $\mathbf{F}_{Vi}(\xi_q, t)$ is expressed as

$$\mathbf{F}_{Vi}(\xi_q, t) = [\mathbf{0} \quad \mathbf{F}_{t_1i}(\xi_q, t) \quad \mathbf{F}_{t_2i}(\xi_q, t)]^T \tag{4a}$$

where

$$\mathbf{F}_{t_ji}(\xi_q, t) = \sum_{m=1}^2 \left\{ \begin{array}{l} k_{1ij}^y Y_{wijm}(\xi_q, t) + c_{1ij}^y \dot{Y}_{wijm}(\xi_q, t) \\ d_{1j}^2 (k_{1ij}^z \theta_{wijm}(\xi_q, t) + c_{1ij}^z \dot{\theta}_{wijm}(\xi_q, t)) - h_{3i} (k_{1ij}^y Y_{wijm}(\xi_q, t) + c_{1ij}^y \dot{Y}_{wijm}(\xi_q, t)) \\ (-1)^{m+1} d_i (k_{1ij}^y Y_{wijm}(\xi_q, t) + c_{1ij}^y \dot{Y}_{wijm}(\xi_q, t)) \\ k_{1ij}^z Z_{wijm}(\xi_q, t) + c_{1ij}^z \dot{Z}_{wijm}(\xi_q, t) \\ (-1)^{m+1} d_i (k_{1ij}^z Z_{wijm}(\xi_q, t) + c_{1ij}^z \dot{Z}_{wijm}(\xi_q, t)) \end{array} \right\} j = 1, 2; \tag{4b}$$

where $Y_{wijm}(\xi_q, t)$, $\theta_{wijm}(\xi_q, t)$, $Z_{wijm}(\xi_q, t)$ are the displacements of the m th wheel set at the j th bogie in the i th car.

2.1.3. Dynamic equation for the bridge model

In the finite element model of the high-speed railway bridge, beams were used that exhibit no shear deformation (i.e. Euler-Bernoulli theory) and satisfy the assumption of a rigid cross-section normal to the longitudinal axis. These assumptions are adequate for this dynamic structural problem. The deformation on the bridge contains bending, shearing, and torsion of the bridge deck, with the deformation of the track components (rail, ballast-less slab track, and concrete seating slab) neglected.

By using the finite element method, the dynamic model of the coupled train-bridge system is shown in Fig. 2, and the linearized system equation of the bridge structure is formulated as

$$\mathbf{M}_b \ddot{\mathbf{X}}_b + \mathbf{C}_b \dot{\mathbf{X}}_b + \mathbf{K}_b \mathbf{X}_b = \mathbf{F}_b(\xi_q, t) \tag{5}$$

where \mathbf{M}_b , \mathbf{C}_b and \mathbf{K}_b are the mass matrix, the damping matrix, and the stiffness matrix of the bridge. The subscript b denotes the bridge. The random parameter set ξ_q in the external random force $\mathbf{F}_b(\xi_q, t)$, which is effect on the bridge, is the factor reflecting the interaction between vehicles and bridge.

Consistent with Ref. [20], the external random force $\mathbf{F}_b(\xi_q, t)$ consists of horizontal forces, vertical forces, and twisting moments, which are transferred by the wheel sets. The forces transferred by the wheel sets consist of two parts, i.e., one is the gravity load distributed by the vehicle and the other is the stochastic interaction triggered by the rail irregularity. In

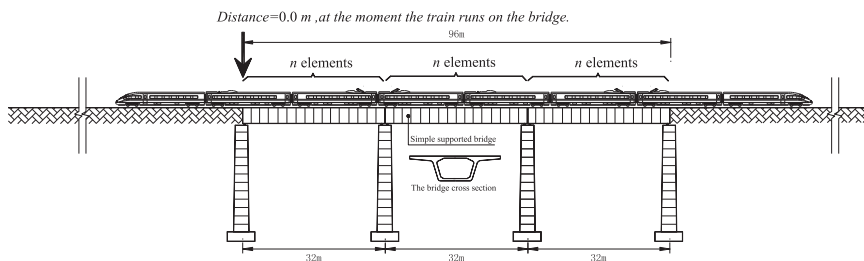


Fig. 2. Finite element model of train-bridge coupled system.

detail, the external stochastic force is expressed as

$$\mathbf{F}_b(\xi_q, t) = \sum_{i=1}^n \sum_{j=1}^2 \sum_{m=1}^2 (F_{yijm}(\xi_q, t) \Phi_{ijm}^y + F_{zijm}(\xi_q, t) \Phi_{ijm}^z + F_{\theta ijm}(\xi_q, t) \Phi_{ijm}^\theta) \quad (6)$$

where Φ_{ijm}^y , Φ_{ijm}^θ and Φ_{ijm}^z correspond to the decomposition-index vectors, by which the internal lateral force, rolling moment and vertical force of the m th wheel-pair in the j th bogie for the i th vehicle acting on the current beam element are decomposed into nodal forces on the element. The external lateral force F_{zijm} , rolling moment $F_{\theta ijm}$ and vertical force F_{yijm} of the m th wheel-set in the j th bogie for the i th vehicle acting on the current bridge beam element are decomposed into nodal forces of the element. The forces are expressed as

$$\begin{cases} F_{yijm}(\xi_q, t) = -m_{wijm} \ddot{Y}_{wijl}(\xi_q, t) + c_{1ij}^y \delta_{t,ijm}^y(\xi_q, t) + k_{1ij}^y \delta_{t,ijm}^y(\xi_q, t) \\ F_{zijm}(\xi_q, t) = g(M_{ci}/4 + M_{tij}/2 + m_{wijm}) - m_{wijm} \ddot{Z}_{wijm}(\xi_q, t) + c_{1ij}^z \delta_{t,ijm}^z(\xi_q, t) + k_{1ij}^z \delta_{t,ijm}^z(\xi_q, t) \\ F_{\theta ijm}(\xi_q, t) = h_{4i} F_{wijm} + e F_{zijm} - J_{wijm} \ddot{\theta}_{wijm}(\xi_q, t) + 2d_{1i}^2 c_{1ij}^z \delta_{t,ijm}^\theta(\xi_q, t) + 2d_{1i}^2 k_{1ij}^z \delta_{t,ijm}^\theta(\xi_q, t) \end{cases} \quad (7)$$

where δ is the relative displacement of the springs between the wheel-sets and the bogies. It is expressed as

$$\begin{cases} \delta_{t,ijm}^y(\xi_q, t) = Y_{t,ij} - h_{3i} \theta_{t,ij} + (-1)^{m+1} d_i \psi_{t,ij} - Y_{wijm}(\xi_q, t) \\ \delta_{t,ijm}^z(\xi_q, t) = Z_{t,ij} + 2(-1)^{m+1} d_i \varphi_{t,ij} - Z_{wijm}(\xi_q, t) \\ \delta_{t,ijm}^\theta(\xi_q, t) = \theta_{t,ij} - \theta_{wijl}(\xi_q, t) \end{cases} \quad (8)$$

2.1.4. Wheel–rail relationship

Based on the above descriptions, a wheel–rail geometrical model is needed for the wheel/rail interaction relationship, which contains the randomness of rail irregularity excitation. It is expressed as follows:

$$\begin{bmatrix} Y_{wjm}(\xi_q, t) \\ \theta_{wjm}(\xi_q, t) \\ Z_{wjm}(\xi_q, t) \end{bmatrix} = \begin{bmatrix} Y_{bijm}(t) + h\theta_{bijm}(t) + Y_{q,N,ijm}(\xi_q, t) \\ \theta_{bijm}(t) + \theta_{q,N,ijm}(\xi_q, t) \\ Z_{bijm}(t) + e\theta_{bijm}(t) + Z_{q,N,ijm}(\xi_q, t) \end{bmatrix} \quad (9)$$

where h and e are the distances from the wheel to the center of a bridge gravity in the z -axis and y -axis respectively, and $Y_{bijm}(t)$, $\theta_{bijm}(t)$, and $Z_{bijm}(t)$ are the bridge displacements that correspond to the location of the wheel at the m th wheel-set of the j th bogie in the i th car.

2.1.5. Vibration of the coupled train–bridge system

By considering the random rail irregularity excitation and referring to the train–bridge model in Refs. [20,27], equations of motion for the coupled train–bridge system, composed of Eqs. (1) and (5), can be expressed in matrix form as follows:

$$\begin{bmatrix} \mathbf{M}_V & \mathbf{0} \\ \mathbf{0} & \mathbf{M}_b \end{bmatrix} \begin{Bmatrix} \ddot{\mathbf{X}}_V \\ \ddot{\mathbf{X}}_b \end{Bmatrix} + \begin{bmatrix} \mathbf{C}_V & \mathbf{0} \\ \mathbf{0} & \mathbf{C}_b \end{bmatrix} \begin{Bmatrix} \dot{\mathbf{X}}_V \\ \dot{\mathbf{X}}_b \end{Bmatrix} + \begin{bmatrix} \mathbf{K}_V & \mathbf{0} \\ \mathbf{0} & \mathbf{K}_b \end{bmatrix} \begin{Bmatrix} \mathbf{X}_V \\ \mathbf{X}_b \end{Bmatrix} = \begin{Bmatrix} \mathbf{F}_V(\xi_q, t) \\ \mathbf{F}_b(\xi_q, t) \end{Bmatrix} \quad (10)$$

The wheel-set degrees of freedom $Y_{wjm}(\xi_q, t)$, $\theta_{wjm}(\xi_q, t)$ and $Z_{wjm}(\xi_q, t)$ in Eq. (10) are not independent, which means these variables are substituted by the wheel–rail relationship in Eq. (9).

Rewrite Eq. (10) in a unified way, one can get the dynamic motion

$$\begin{bmatrix} \mathbf{M}_V & \mathbf{0} \\ \mathbf{0} & \mathbf{M}'_b \end{bmatrix} \begin{Bmatrix} \ddot{\mathbf{X}}_V \\ \ddot{\mathbf{X}}_b \end{Bmatrix} + \begin{bmatrix} \mathbf{C}_V & \mathbf{C}'_{Vb} \\ \mathbf{C}_{bV} & \mathbf{C}'_b \end{bmatrix} \begin{Bmatrix} \dot{\mathbf{X}}_V \\ \dot{\mathbf{X}}_b \end{Bmatrix} + \begin{bmatrix} \mathbf{K}_V & \mathbf{K}'_{Vb} \\ \mathbf{K}_{bV} & \mathbf{K}'_b \end{bmatrix} \begin{Bmatrix} \mathbf{X}_V \\ \mathbf{X}_b \end{Bmatrix} = \mathbf{F}_g + \mathbf{F}_\phi(\xi_q, t) \quad (11)$$

where \mathbf{M}'_b , \mathbf{C}'_{Vb} and \mathbf{K}'_{Vb} are the hybrid matrices associated with bridge structure matrices and shape function matrices with the contribution of wheel-sets forces. \mathbf{K}_{Vb} and \mathbf{C}_{Vb} are the hybrid matrices associated with bridge deflection and wheel-sets forces. These matrices are written as

$$\mathbf{M}'_b = \mathbf{M}_b + \sum_{i=1}^n \sum_{j=1}^2 \sum_{m=1}^2 (m_{wijm} \Phi_{ijm}^y \Phi_{ijm}^{yT} + m_{wijm} \Phi_{ijm}^z \Phi_{ijm}^{zT} + J_{wijm} \Phi_{ijm}^\theta \Phi_{ijm}^{\theta T}) \quad (12a)$$

$$\mathbf{K}'_b = \mathbf{K}_b + \sum_{i=1}^n \sum_{j=1}^2 \sum_{m=1}^2 (k_{1ij}^y \Phi_{ijm}^y \Phi_{ijm}^{yT} + k_{1ij}^z \Phi_{ijm}^z \Phi_{ijm}^{zT} + d_{1i}^2 k_{1ij}^z \Phi_{ijm}^\theta \Phi_{ijm}^{\theta T}) \quad (12b)$$

$$\mathbf{K}_{Vb} = \mathbf{K}'_{bV} = [\mathbf{K}_{Vb1}, \mathbf{K}_{Vb2}, \dots, \mathbf{K}_{Vbn}]^T \quad (12c)$$

$$\mathbf{K}_{Vbi} = [\mathbf{0}, \mathbf{K}_{t_1b}^i, \mathbf{K}_{t_2b}^i]^T, \mathbf{K}_{t_jb}^i = - \begin{bmatrix} k_{1ij}^y \Phi_{ijm}^{yT} \\ d_{1i}^2 k_{1ij}^z \Phi_{ijm}^{zT} - h_{3i} k_{1ij}^y \Phi_{ijm}^{yT} \\ (-1)^j d_i k_{1ij}^y \Phi_{ijm}^{yT} \\ k_{1ij}^z \Phi_{ijm}^{zT} \\ (-1)^j d_i k_{1ij}^z \Phi_{ijm}^{zT} \end{bmatrix}, j = 1, 2 \quad (12d)$$

$$\Phi_{ijm}^y = \Phi_{ijm}^y + h_{4i} \Phi_{ijm}^\theta; \Phi_{ijm}^z = \Phi_{ijm}^z + e \Phi_{ijm}^\theta \quad (12e)$$

The matrices \mathbf{C}_b^c , \mathbf{C}_{Vb} and \mathbf{C}_{bv} have the same form as \mathbf{K}_b^c , \mathbf{K}_{Vb} and \mathbf{K}_{bv} . By replacing \mathbf{K} with \mathbf{C} and k with c , we can obtain the matrices \mathbf{C}_b^c , \mathbf{C}_{Vb} and \mathbf{C}_{bv} .

\mathbf{F}_g represents the deterministic excitation vector due to gravitational load on the cars. $\mathbf{F}_\phi(\xi_q, t)$ is the three-dimensional, random non-stationary excitation vector caused by the lateral, rotational, and vertical rail irregularities that are generated with stochastic harmonic function mentioned in Section 2. The excitation forces \mathbf{F}_g and $\mathbf{F}_\phi(\xi_q, t)$ can be expressed as

$$\mathbf{F}_g = \left[\mathbf{0} \quad \sum_{i=1}^n \sum_{j=1}^2 \sum_{l=1}^2 g(M_{ci}/4 + M_{tij}/2 + m_{wijm}) \Phi_{ijm}^z \right]^T \quad (13)$$

$$\mathbf{F}_\phi(\xi_q, t) = \mathbf{K}_F \mathbf{U}_w(\xi_q, t) + \mathbf{C}_F \dot{\mathbf{U}}_w(\xi_q, t) + \mathbf{M}_F \ddot{\mathbf{U}}_w(\xi_q, t) \quad (14)$$

where the random rail irregularity matrices $\dot{\mathbf{U}}_w(\xi_q, t)$ and $\ddot{\mathbf{U}}_w(\xi_q, t)$ have the same form as $\mathbf{U}_w(\xi_q, t)$ in Eq. (14) except for the time derivative. The response matrix $\mathbf{U}_w(\xi_q, t)$ is expressed as

$$\mathbf{U}_w(\xi_q, t) = [\mathbf{U}_{w1}, \mathbf{U}_{w2}, \dots, \mathbf{U}_{wN}]^T, \mathbf{U}_{wi} = [\mathbf{U}_{wi}^{11}, \mathbf{U}_{wi}^{12}, \mathbf{U}_{wi}^{21}, \mathbf{U}_{wi}^{22}]^T \\ \mathbf{U}_{wi}^{jm} = [Y_{q,N,ijm}(\xi_q, t) \quad \theta_{q,N,ijm}(\xi_q, t) \quad Z_{q,N,ijm}(\xi_q, t)]^T \quad (15a)$$

Similarly, matrices \mathbf{K}_F and \mathbf{M}_F in Eq. (14) are rewritten in Eqs. (15b)–(15d). The damping matrix \mathbf{C}_F has the same form as the stiff matrix \mathbf{K}_F . The subscripts are $i = 1, 2, \dots, n, j = 1, 2$, and $m = 1, 2$.

$$\mathbf{K}_F = [\mathbf{K}_{FV} \quad \mathbf{K}_{Fb}]^T, \mathbf{K}_{FV} = \text{diag}[\mathbf{K}_{FV1}, \mathbf{K}_{FV2}, \dots, \mathbf{K}_{FVN}] \\ \mathbf{K}_{FVi} = \begin{bmatrix} \mathbf{0} & \mathbf{0} & \mathbf{0} & \mathbf{0} \\ \mathbf{K}_{FVi}^{11} & \mathbf{K}_{FVi}^{12} & \mathbf{0} & \mathbf{0} \\ \mathbf{0} & \mathbf{0} & \mathbf{K}_{FVi}^{21} & \mathbf{K}_{FVi}^{22} \end{bmatrix}, \mathbf{K}_{FVi}^{jm} = \begin{bmatrix} 2k_{1ij}^y & -2k_{1ij}^y h_{3i} & (-1)^{m+1} 2k_{1ij}^y d_i & 0 & 0 \\ 0 & 2k_{1ij}^z d_{1i}^2 & 0 & 0 & 0 \\ 0 & 0 & 0 & 2k_{1ij}^z & (-1)^{m+1} 2k_{1ij}^z d_i \end{bmatrix}^T \quad (15b)$$

$$\mathbf{K}_{Fb} = [\mathbf{K}_{Fb1}, \mathbf{K}_{Fb2}, \dots, \mathbf{K}_{Fbn}], \mathbf{K}_{Fbi} = [\mathbf{K}_{Fbi}^{11}, \mathbf{K}_{Fbi}^{12}, \mathbf{K}_{Fbi}^{21}, \mathbf{K}_{Fbi}^{22}] \\ \mathbf{K}_{Fbi}^{jm} = \begin{bmatrix} -k_{1ij}^y (\Phi_{ijm}^y + h_{4i} \Phi_{ijm}^\theta) & -d_{1i}^2 k_{1ij}^z \Phi_{ijm}^\theta & -k_{1ij}^z (\Phi_{ijm}^z + e \Phi_{ijm}^\theta) \end{bmatrix} \quad (15c)$$

$$\mathbf{M}_F = [\mathbf{0} \quad \mathbf{M}_{Fb}]^T, \mathbf{M}_{Fb} = [\mathbf{M}_{Fb1}, \mathbf{M}_{Fb2}, \dots, \mathbf{M}_{Fbn}], \mathbf{M}_{Fbi} = [\mathbf{M}_{Fbi}^{11}, \mathbf{M}_{Fbi}^{12}, \mathbf{M}_{Fbi}^{21}, \mathbf{M}_{Fbi}^{22}] \\ \mathbf{M}_{Fbi}^{jm} = \begin{bmatrix} -m_{wijm} (\Phi_{ijm}^y + h_{4i} \Phi_{ijm}^\theta) & -J_{wijm} \Phi_{ijm}^\theta & -m_{wijm} (\Phi_{ijm}^z + e \Phi_{ijm}^\theta) \end{bmatrix} \quad (15d)$$

2.2. Stochastic harmonic functions of rail irregularity

2.2.1. Sample simulation and representative point selection

After building the dynamic train–bridge model, the key point of next step is the generation of random rail irregularity samples. As the time–history curves, rail irregularity samples are generated for numerical simulation of the train–bridge system. It is common to use the rail irregularity samples generated by numerical method for simulation rather than those measured according to the actual condition. In this study, a stochastic harmonic function (SHF) [25] was employed to generate random rail irregularity from the rail irregularity power spectrum density that contains random spatial frequencies, phases, and amplitudes that are determined by spatial frequencies. With this method, power spectrum density of the generated rail irregularity samples is precisely equivalent to the original one [22].

Track alignment irregularity, track vertical profile irregularity and track cross-level irregularity are expressed as $y_N(\Theta, x)$, $\theta_N(\Theta, x)$ and $z_N(\Theta, x)$ respectively, which are shown in Fig. 3. As mentioned in Ref. [22], $\Omega_{\theta,i}^l$ and $\phi_{\theta,i}^l$ ($i = 1, 2, \dots, N, l = y, u, z$) are considered as the spatial frequency and phase angle of rail irregularity respectively, and they are evenly distributed at the interval value of $(\Omega_{i-1}^{(p)}, \Omega_i^{(p)})$ and in period of $(0, 2\pi)$ independently. Here, Θ is considered to be a random variable vector set, and $\Omega_i^{(p)}$ is the dividing frequency that meets the interval domain $\Omega_l < \Omega_1^{(p)} < \Omega_2^{(p)} < \dots < \Omega_{N-1}^{(p)} < \Omega_u$, Ω_u is the upper cut-off spatial frequency and Ω_l is the lower cut-off spatial frequency. The power spectrum density values of rail irregularity change exponentially within the domain of the cut-off frequencies, a feature that is different from the

earthquake spectrum density and the wind load spectrum density. Therefore, it is important to ensure that $\Omega_i^{(p)}$ is credible for the simulation. The rail irregularity samples that generated by SHF are expressed as

$$\begin{cases} y_N(\Theta, x) = \sum_{i=1}^N A_y(\Omega_{\theta,i}^y) \cos(\Omega_{\theta,i}^y x + \phi_{\theta,i}^y) \\ \theta_N(\Theta, x) = \sum_{i=1}^N A_u(\Omega_{\theta,i}^u) \cos(\Omega_{\theta,i}^u x + \phi_{\theta,i}^u) \\ z_N(\Theta, x) = \sum_{i=1}^N A_z(\Omega_{\theta,i}^z) \cos(\Omega_{\theta,i}^z x + \phi_{\theta,i}^z) \end{cases} \quad (16)$$

where amplitude $A_I(\Omega_{\theta,i}^I)$ is a function of $\Omega_{\theta,i}^I$, $I = y, u, z$, and N is the number of components.

The greater the number N is, the higher accuracy of the power spectral density function (PSDs) of stochastic harmonic function process has, as compared to the target power spectral density [28]. The minimum value of N used for the frequency truncation, which ensures enough precision for calculation, could be $N = 10$ with stochastic harmonic function, according to Ref. [28]. In this study, the number $N = 50$ was chosen, which would be accurate enough in generating rail irregularity samples.

$S_I(\Omega_{\theta,i}^I)$ is set as PSDs of rail irregularity (see Ref. [24]) and the amplitude $A_I(\Omega) = \sqrt{2S_I(\Omega_{\theta,i}^I)\Delta\Omega_{\theta,i}^I\pi^{-1}}$, $I = y, u, z$. Thus, Eq. (16) becomes

$$\begin{cases} y_N(\Theta, x) = \sum_{i=1}^N \sqrt{2S_y(\Omega_{\theta,i}^y)\Delta\Omega_{\theta,i}^y\pi^{-1}} \cos(\Omega_{\theta,i}^y x + \phi_{\theta,i}^y) \\ \theta_N(\Theta, x) = \sum_{i=1}^N \sqrt{2S_u(\Omega_{\theta,i}^u)\Delta\Omega_{\theta,i}^u\pi^{-1}} \cos(\Omega_{\theta,i}^u x + \phi_{\theta,i}^u) \\ z_N(\Theta, x) = \sum_{i=1}^N \sqrt{2S_z(\Omega_{\theta,i}^z)\Delta\Omega_{\theta,i}^z\pi^{-1}} \cos(\Omega_{\theta,i}^z x + \phi_{\theta,i}^z) \end{cases} \quad (17)$$

where $\Omega_{\theta,i}^I$, $I = y, \theta, z$ is the spatial frequency of rail irregularity. The relationship between this frequency and circular frequency ω is $\omega_{\theta,i}^I = \Omega_{\theta,i}^I v = 2\pi v / \lambda_{\theta,i}^I$, where v is the train speed and λ is the rail irregularity wavelength. The PSDs of stochastic process $y_N(\Theta, x)$, $\theta_N(\Theta, x)$ and $z_N(\Theta, x)$ are precisely equal to the original PSD [22] when all these conditions are met.

Furthermore, to obtain the representative samples of random function which contain probability information, the number theoretical method (NTM) [29,30] with $2N$ dimensional spatial vectors is employed to select random spatial frequency points that were used to generate the random track irregularity samples.

A $2N$ dimensional hypercube point set (gp set, one mentioned in NTM) is generated by using the square root method of sequence:

$$X_{q,i} = \{q\sqrt{\varpi_i}\} \quad (18)$$

where $q = 1, 2, \dots, n_{pt}$, $i = 1, 2, \dots, 2N$, $X_{q,i} \in (0, 1)$ is the evenly scattered point set of a $2N$ dimensional hypercube, ϖ_i are different prime numbers, $\{\cdot\}$ shows the decimal part of $q\sqrt{\varpi_i}$, and n_{pt} is the total number of representative rail irregularity samples.

Researchers [22] have suggested that the variable ϖ_i in Eq. (18) be a prime number equal to the i th ($i = 1, 2, \dots, 2N$) prime number in turn, and the prime numbers are presented in a prime number sequence at first. The discrete representative

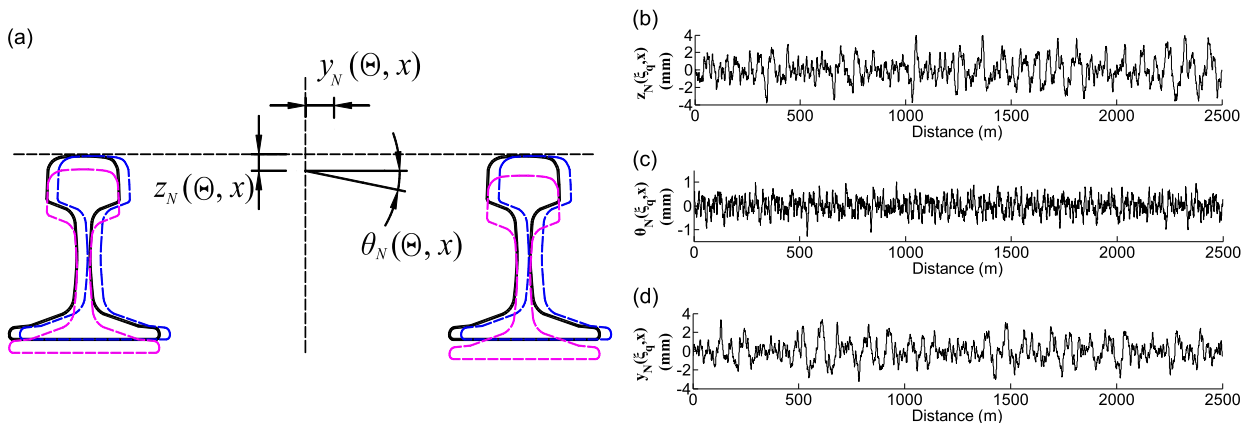


Fig. 3. Random geometric track irregularities simulated with stochastic harmonic functions: (a) abridged general view of railway rail irregularity; (b) track vertical profile irregularity; (c) track cross-level irregularity; and (d) track alignment irregularity.

points are shown as

$$\begin{cases} (\tilde{\Omega}_{q,i})^{-1} = (\Omega_{i-1}^{(p)})^{-1} + [(\Omega_{i-1}^{(p)})^{-1} - (\Omega_i^{(p)})^{-1}] \chi_{q,i} \\ \tilde{\phi}_{q,i} = 2\pi\chi_{q,i+N} \end{cases} \quad (19)$$

where $q = 1, 2, \dots, n_{pt}$, $i = 1, 2, \dots, N$ and $j = 1, 2, \dots, N$.

In particular, $\Omega_i^{(p)}$ in Eq. (19) is the dividing frequency which is met in the intervals $\Omega_1 < \Omega_1^{(p)} < \Omega_2^{(p)} < \dots < \Omega_{N-1}^{(p)} < \Omega_N$, $\tilde{\Omega}_{q,i}$ is the i th adjusted random spatial frequency of q th random vector sets, and $\tilde{\phi}_{q,i}$ is the $i+N$ th adjusted random phase angle of q th random vector set.

The random vector set ξ_q is expressed as $\xi_q = (\tilde{\Omega}_{q,1}, \tilde{\Omega}_{q,2}, \dots, \tilde{\Omega}_{q,N}, \tilde{\phi}_{q,1}, \tilde{\phi}_{q,2}, \dots, \tilde{\phi}_{q,N}) \in \Theta$, and its joint probability density function is considered to be $p_{\Theta}(\xi_q)$, whose initial probability assignment is $P_q = 1/n_{pt}$.

Substituting Eq. (19) into Eq. (17) yields

$$\begin{cases} \tilde{y}_{q,N}(\xi_q, x) = \sum_{i=1}^N \sqrt{2S_y(\tilde{\Omega}_{q,i}^y)\Delta\tilde{\Omega}_{q,i}^y\pi^{-1}} \cos(\tilde{\Omega}_{q,i}^y x + \tilde{\phi}_{q,i}^y) \\ \tilde{\theta}_{q,N}(\xi_q, x) = \sum_{i=1}^N \sqrt{2S_y(\tilde{\Omega}_{q,i}^u)\Delta\tilde{\Omega}_{q,i}^u\pi^{-1}} \cos(\tilde{\Omega}_{q,i}^u x + \tilde{\phi}_{q,i}^u) \\ \tilde{z}_{q,N}(\xi_q, x) = \sum_{i=1}^N \sqrt{2S_y(\tilde{\Omega}_{q,i}^z)\Delta\tilde{\Omega}_{q,i}^z\pi^{-1}} \cos(\tilde{\Omega}_{q,i}^z x + \tilde{\phi}_{q,i}^z) \end{cases} \quad (20)$$

where $q = 1, 2, \dots, n_{pt}$.

2.2.2. Rail irregularity time domain transformation and non-stationary modulation

Rail irregularity cannot generally be assumed to be stationary for a train crossing a bridge, and the amplitude of rail irregularity on the bridge is normally smaller than the amplitude in the subgrade layer. On such a basis, it was assumed that the PSD values of rail irregularity on the bridge were $c = 0.7$ times lower than those in the subgrade layer.

Let $\Phi_l(x)(l = y, \theta, z)$ be a slowly varying sinusoidal modulation function for track alignment irregularity, track vertical profile irregularity, and track cross-level irregularity, respectively. As mentioned in Ref. [20], the transformation function is given as

$$\Phi_l(x) = \begin{cases} 0.5(1 + \sqrt{c}) + 0.5(1 - \sqrt{c})\sin(\pi L_0^{-1}(x + 1.5L_0)) & -L_0 \leq x < 0 \\ \sqrt{c} & 0 \leq x < L \\ 0.5(1 + \sqrt{c}) + 0.5(1 - \sqrt{c})\sin(\pi L_0^{-1}(x - L - 0.5L_0)) & L \leq x < L + L_0 \\ 1 & \text{other} \end{cases} \quad (21)$$

where L_0 is the length of the transition section before the train enters the bridge, and L is the total length of bridge.

Based on the conversation relationship of $x = vt$, rail irregularity samples generated by SHF can be expressed as time-domain curves that are shown as follows:

$$\begin{cases} Y_{q,N}(\xi_q, t) = \Phi_y(vt)\tilde{y}_{q,N}(\xi_q, vt) \\ \theta_{q,N}(\xi_q, t) = \Phi_\theta(vt)\tilde{\theta}_{q,N}(\xi_q, vt) \\ Z_{q,N}(\xi_q, t) = \Phi_z(vt)\tilde{z}_{q,N}(\xi_q, vt) \end{cases} \quad (22)$$

2.3. Solution of the dynamic equation using probability density evolution method

Without loss of generality, the dynamic train–bridge equation in Eq. (11) can be rewritten as

$$M\ddot{\mathbf{X}}(\Theta, t) + C\dot{\mathbf{X}}(\Theta, t) + \mathbf{K}\mathbf{X}(\Theta, t) = \mathbf{F}(\Theta, t) \quad (23)$$

To express the random factors more clearly, the random variable Θ was replaced with the variable set ξ_q in Eq. (23), where $\xi_q \in \Theta, q = 1, 2, \dots, n_{pt}$. Random rail irregularity is considered to be the only random excitation source in Eq. (23); Further, the dynamic train–bridge system is also assumed to be a conservative system. Therefore, the randomness of the dynamic equation comes from the random parameter set Θ [23].

In that case, for conciseness and greater clarity, Eq. (23) can be rewritten as

$$M\ddot{\mathbf{X}}(\xi_q, t) + C\dot{\mathbf{X}}(\xi_q, t) + \mathbf{K}\mathbf{X}(\xi_q, t) = \mathbf{F}(\xi_q, t) \quad (24)$$

The steps in the calculation of the dynamic train–bridge system with PDEM are listed as follows:

Step 1 Select the representative points in the random parameter space Θ . The sample set of representative random spatial frequencies that are used to generate random track irregularity samples is filtered with NTM (Eqs. (18) and (19)).

The initial probability of each parameter set is denoted as P_q , and the total probability of train–bridge system satisfies:

$$\sum_{q=1}^{n_{pt}} P_q = \sum_{q=1}^{n_{pt}} \int_{\xi_q} p_{\Theta}(\xi_q) d\xi = \int_{\cup_{q=1}^{n_{pt}} \xi_q} p_{\Theta}(\xi_q) d\xi = \int_{\Omega_{\Theta}} p_{\Theta}(\xi_q) d\xi = 1 \tag{25}$$

The initial conditions are partially discretized correspondingly as

$$p_{U\Theta}(u, \xi_q, t)|_{t=t_0} = \delta(u - u_0) p_{\Theta}(\xi_q, t)|_{t=t_0} = \delta(u - u_0) P_q \tag{26}$$

where $\delta(\cdot)$ is a Dirac delta function.

Step 2 Perform the deterministic structural analysis of the train–bridge system in Eq. (23) within the prescribed $\Theta = \xi_q (q = 1, 2, \dots, n_{pt})$ using the *Newmark–β* step-by-step integration method and output the random responses matrices $\mathbf{X}(\xi_q, t)$, $\dot{\mathbf{X}}(\xi_q, t)$ and $\ddot{\mathbf{X}}(\xi_q, t)$. The samples of rail irregularity are generated within the prescribed $\Theta = \xi_q$.

Step 3 Replace the random responses $\mathbf{X}(\xi_q, t)$, $\dot{\mathbf{X}}(\xi_q, t)$ and $\ddot{\mathbf{X}}(\xi_q, t)$ with the variable \mathbf{U} . The variable \mathbf{U} is rewritten as

$$\mathbf{U}(\xi_q, t) = [\mathbf{X}(\xi_q, t)^T \quad \dot{\mathbf{X}}(\xi_q, t)^T]^T \tag{27}$$

The train–bridge dynamic equation in Eq. (23) can be rewritten as

$$\dot{\mathbf{U}}(\xi_q, t) = \mathbf{A}\mathbf{U}(\xi_q, t) + \mathbf{Q}(\xi_q, t) \tag{28}$$

where

$$\mathbf{A} = \begin{bmatrix} \mathbf{0} & \mathbf{I} \\ -\mathbf{M}^{-1}\mathbf{K} & -\mathbf{M}^{-1}\mathbf{C} \end{bmatrix}, \quad \mathbf{Q}(\xi_q, t) = \begin{bmatrix} \mathbf{0} \\ \mathbf{M}^{-1}\mathbf{F}(\xi_q, t) \end{bmatrix}$$

The component form of \mathbf{U} is

$$\dot{U}_l(\xi_q, t) = \sum_{j=1}^{2N} A_{lj} U_j(\xi_q, t) + Q_l(\xi_q, t) \quad (l = 1, 2, \dots) \tag{29}$$

Based on the *Reynold* transformation theorem and its related derivation, the generalized probability density evolution equation (GPDEE) [23] is obtained as follows:

$$\frac{\partial p_{U\Theta}(u, \xi_q, t)}{\partial t} + \dot{U}_l(\xi_q, t) \frac{\partial p_{U\Theta}(u, \xi_q, t)}{\partial u} = 0 \tag{30}$$

where $\dot{U}_l(\xi_q, t)$ is the time rate of the dynamic train–bridge response $\mathbf{U}_l(t)$ with $\{\Theta = \xi_q\}$.

Step 4 The GPDEE of the train–bridge random system Eq. (30) is solved together with Eq. (24). The bilateral difference method with the functionality of total variation diminishing (TVD) format [22] is used to solve the partial differential equation Eq. (30) and obtain the solution $p_{U\Theta}(u, \xi_q, t)$.

The PDF of the dynamic train–bridge system response is given by

$$p_{\mathbf{U}}(u, t) = \int_{\Theta} p_{U\Theta}(u, \xi_q, t) d\xi \tag{31}$$

More details are referred to reference [22].

3. Numerical examples and validation

3.1. General information

A three-dimensional (3D) dynamic coupled train–bridge system was established to evaluate the interaction models in high-speed railways, as shown in Fig. 1. The bridge was composed of three simply supported beams. Each beam is a pre-stressed concrete box girder spanning 32 m and the box section is shown in Fig. 2. Each beam is modeled as 20 spatial finite beam elements. Referring to the coordinate system built in Fig. 1, one of the bridge deck ends is fixed in the x, y, z , and θ_x directions, and at the other end y, z , and θ_x are constrained. The piers of the bridge are assumed to be rigid and are neglected in the finite element model. The mechanical parameters of the bridge are listed in Table 1.

The German ICE-3 train is composed of eight passenger cars of which the 1st and 8th are locomotives. The mechanical parameters of the cars are shown in Table 2.

The MATLAB[®] package, a commercial data-analysis and visualization tool, was used to compile the train–bridge random vibration program. This program was based on PDEM with random rail irregularity as the excitation source. Comparisons between the current method and MCM are also presented and discussed.

3.2. Verification of computational efficiency and accuracy

In this study, rail irregularity is considered the only excitation source for the train–bridge vibration system in the analysis. For better understanding of the dynamic system, various combinations of rail irregularity excitation were used in the simulation. Four different combinations were considered, including vertical profile track irregularity, cross-level track irregularity, track alignment irregularity and the combined track irregularities.

Previous research work has mainly focused on the deterministic analysis of the coupled train–bridge vibration [2,15,16], which is not adequate for revealing the physical mechanisms of the random vibration of the train–bridge system. It has been proved that responses of the system have considerable differences when only one or a few samples of measured or simulated rail irregularity excitation are used. Previous studies did not systematically investigate random vibration of the train–bridge system, although the classic MCM is appropriate but comes with huge computational cost. In this study, the MCM was used to verify the reliability of other competing methods.

The PDEM has higher efficiency than MCM for the same accuracy level and was used to calculate the random vibration of the train–bridge system. The computed responses of the system in the vertical direction are presented in Figs. 4–6. As for Figs. 4–6, the 3D probability density surfaces shown in the (a) figures are the time–history curves for the bridge acceleration, vehicle displacement, and vehicle acceleration. The sectional area of each time step is always equal to 1 because there is no

Table 1
Calibrated mechanical properties of the bridge section.

Item	Unit	Value
\bar{m} (mass per unit length)	kg/m	22,197.2
EI_z (lateral bending stiffness)	GPa m ⁴	2963.8
EI_y (vertical bending stiffness)	GPa m ⁴	377.4
$I_0 = I_y + I_z$ (the polar inertia)	m ⁴	96.8
GI_t (the torsional stiffness)	GPa m ⁴	289.8

Table 2
Major parameters of the vehicle used in the present study.

Parameters for the <i>i</i> th vehicle	Unit	Tractor	Trailer
M_{ci} (mass of body)	kg	48,000	44,000
J_{cxi} (roll mass moment of body)	kg m ²	115,000	100,000
J_{cpi} (yaw mass moment of body)	kg m ²	2,700,000	2,700,000
J_{cxi} (pitch mass moment of body)	kg m ²	2,700,000	2,700,000
M_{tij} (mass of bogie)	kg	3200	2400
J_{tixj} (roll mass moment of bogie)	kg m ²	3200	2400
J_{tpij} (yaw mass moment of bogie)	kg m ²	6800	6800
J_{tpij} (pitch mass moment of bogie)	kg m ²	7200	7200
m_{wijn} (mass of wheel-pair)	kg	2400	2400
J_{wijk} (roll mass moment of wheel-pair)	kg m ²	1200	1200
k_{1ij}^z (vertical stiffness of 1st suspension system, per side)	kN/m	1,040,000	700,000
k_{1ij}^y (lateral stiffness of 1st suspension system, per side)	kN/m	3,000,000	5,000,000
k_{2ij}^z (vertical stiffness of 2nd suspension system, per side)	kN/m	400,000	300,000
k_{2ij}^y (lateral stiffness of 2nd suspension system, per side)	kN/m	480,000	560,000
c_{1ij}^z (vertical damping of 1st suspension system, per side)	kN s/m	50	50
c_{1ij}^y (lateral damping of 1st suspension system, per side)	kN s/m	30	30
c_{2ij}^z (vertical damping of 2nd suspension system, per side)	kN s/m	60	60
c_{2ij}^y (lateral damping of 2nd suspension system, per side)	kN s/m	30	25
L_{ci} (full length of vehicle)	m	24.775	24.775
s_i (half-distance of two bogies)	m	17.375/2	17.375/2
d_i (half-distance of two wheel-pairs)	m	1.25	1.25
d_{1i} (half-span of the 1st suspension system)	m	1.00	1.00
d_{2i} (half-span of the 2nd suspension system)	m	0.95	0.95
b_{ijk} (half-span of the wheel-pair)	m	1.496/2	1.496/2
e (lateral distance from wheel-set to bridge center)	m	2.50	2.50
h (vertical distance from rail to bridge center)	m	1.80	1.80
h_{1i} (height of body above 2nd suspension system)	m	0.80	0.80
h_{2i} (height of 2nd suspension system above bogie)	m	0.30	0.20
h_{3i} (height of bogie above wheel-pair)	m	−0.05	0.10
h_{4i} (height of wheel-pair above bridge centroid)	m	2.30	2.30

probability loss enduring the whole process. The probability density contours of these responses are displayed in the (b) figures. The curves for mean and standard deviation values are displayed in the (c) and (d) figures, respectively.

3.2.1. Bridge acceleration

In Fig. 4(a) and (b), the probability density of bridge acceleration at the mid-span is concentrated at the initial distance of 0.0 m where the train starts to enter the bridge, and then spreads gradually until reaching a maximum at each wave crest. After the train leaves the bridge, the probability density returns to the initial position. This phenomenon is consistent with the actual condition in the coupled train–bridge vibration.

The mean value curve in Fig. 4(c) and standard deviation curve in Fig. 4(d) show that the vertical bridge acceleration at mid-span is greatly influenced by the random vertical profile track irregularity, and that the largest coefficient of variation for the acceleration in Fig. 4 reaches 16.92 percent. The coefficient of variation for bridge acceleration is calculated as the standard deviation in Fig. 4(d) divided by the average value at each peak in Fig. 4(c).

The MCM is considered as a method of validation for the high efficiency of PDEM at the same accuracy level. The statistical result of 5000 samples generated by MCM is close to the result calculated by PDEM with 300 representative samples. The maximum deviation is within 2.11 percent at the distance of 220 m that corresponds to the exact time point when train leaves the bridge. However, the computation time of the MCM is almost 18 times more than that of PDEM. This demonstrates that the computational efficiency of PDEM is much higher than that of MCM, for the same accuracy level.

3.2.2. Vehicle displacement and acceleration

Due to the random vertical profile track irregularity, the responses of vehicle showed greater randomness than those of bridge structure. The response curves in Figs. 5 and 6 show the response of vehicle at a train speed of 240 km/h. The peak areas in Figs. 5(a) and 6(a) are mainly distributed within the distance from 0 to 100 m, which implies that the train runs more stably on the bridge than on the embankment.

The mean value curve of vertical vehicle displacement at the center of gravity is shown in Fig. 5(c). The curve decreases at the beginning and rises between 0 m and 100 m because of the coupled train–bridge vibration. The standard deviation curves in Fig. 5(d) show similar trend as the mean value curves in Fig. 5(c), however, their mechanisms are different from each other. The mean value curves in Fig. 5(c) descends due to the action of vehicle gravity when running across the bridges, while the standard deviation curves in Fig. 5(d) descends due to the modulation of the rail irregularity that has been introduced to take into account the fact that rail irregularity on the bridge is generally smaller than that on the embankment. Therefore, when train runs on the bridges, the standard deviation of vertical car-body displacement is smaller than that on the subgrade. The ratio of minimum and maximum values of the curves in Fig. 5(d) is 0.62, close to the modulation rate 0.7.

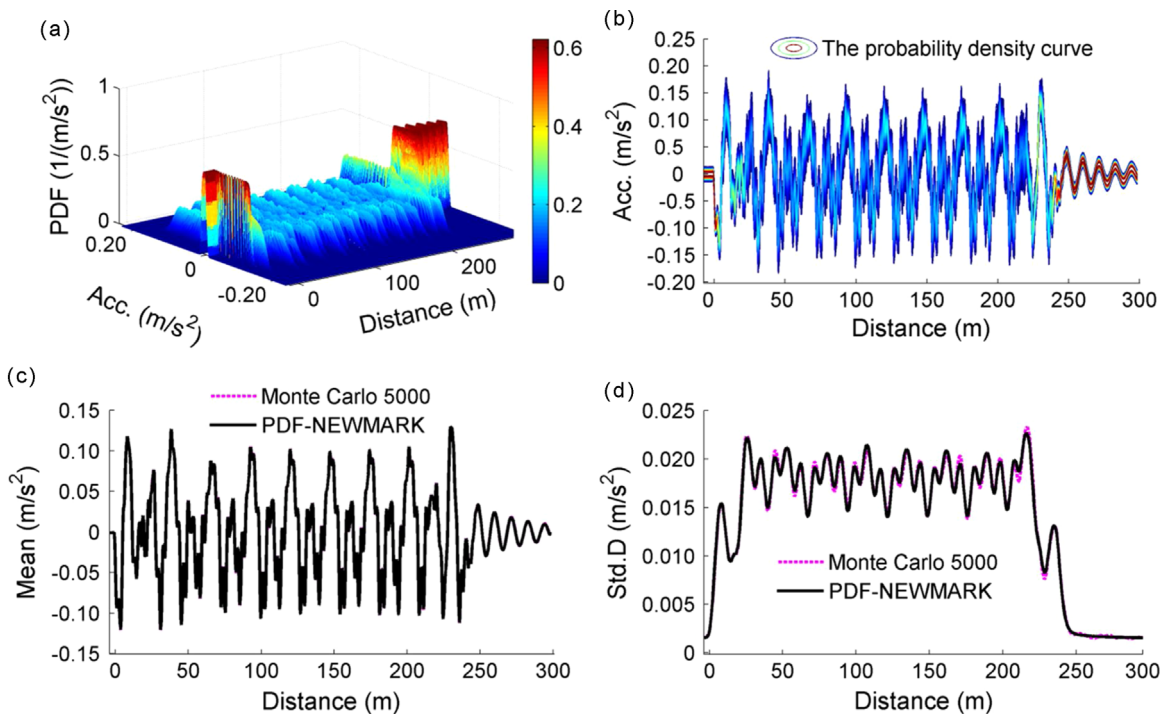


Fig. 4. Random vertical acceleration histories at the bridge midspan under random vertical profile track irregularity ($v=240$ km/h): (a) 3D probability density evolution surface; (b) probability density contour curve; (c) mean value curve; and (d) standard deviation curve.

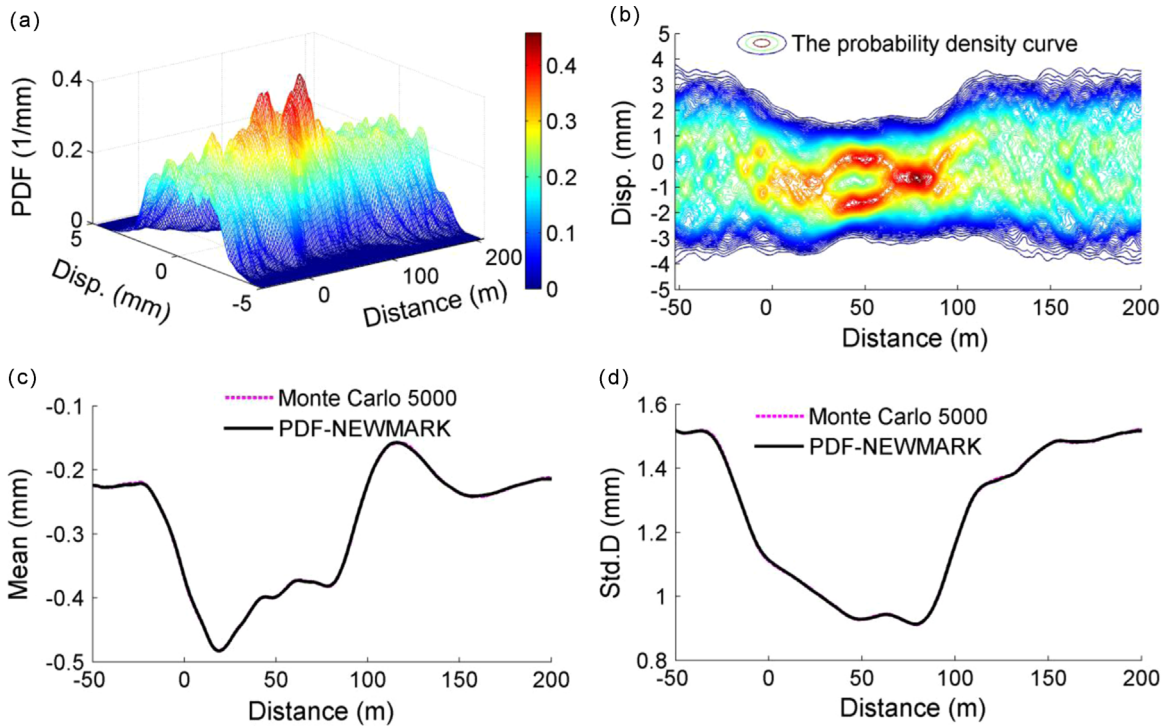


Fig. 5. Random vertical displacement histories at the gravity center of the first car-body under random vertical profile track irregularity ($v=240$ km/h): (a) 3D probability density evolution surface; (b) probability density contour curve; (c) mean value curve; and (d) standard deviation curve.

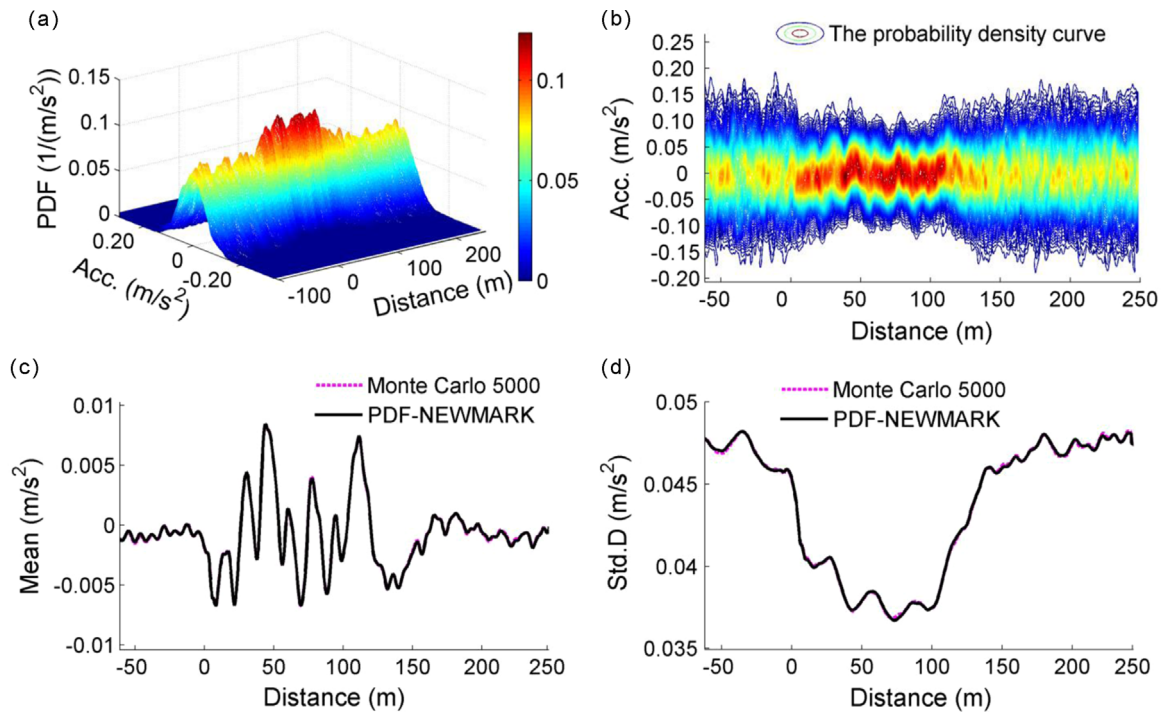


Fig. 6. Random vertical acceleration histories at the gravity center of the first car-body under random vertical profile track irregularity ($v=240$ km/h): (a) 3D probability density evolution surface; (b) probability density contour curve; (c) mean value curve; and (d) standard deviation curve.

The vertical vehicle acceleration curves at the center of gravity shown in Fig. 6 are consistent with those in Fig. 5. The MCM was used to test the efficiency and precision of PDEM. The curves obtained using PDEM and MCM matched well, with the former using 300 representative samples and the latter using 5000 samples. The maximum deviation is within 1.92 percent. This again proves that the PDEM has higher efficiency than the MCM for the same accuracy level.

3.3. Analysis of vibration response and influence of speed

Bridge resonance is a common concern in the vibration of a train–bridge system. It is detrimental when the bridge resonance occurs at the time a train is running across the bridge at a particular speed. To study the random vibration of the train–bridge system at different train speeds, four different types of track irregularity were used in the calculation, i.e., vertical profile track irregularity (vertical only), cross-level track irregularity (rotational only), track alignment irregularity (alignment only), and the three track irregularities combined (all combined). The train speed values were divided into 13 levels ranging between 60 km/h and 420 km/h with an increment of 30 km/h for each level.

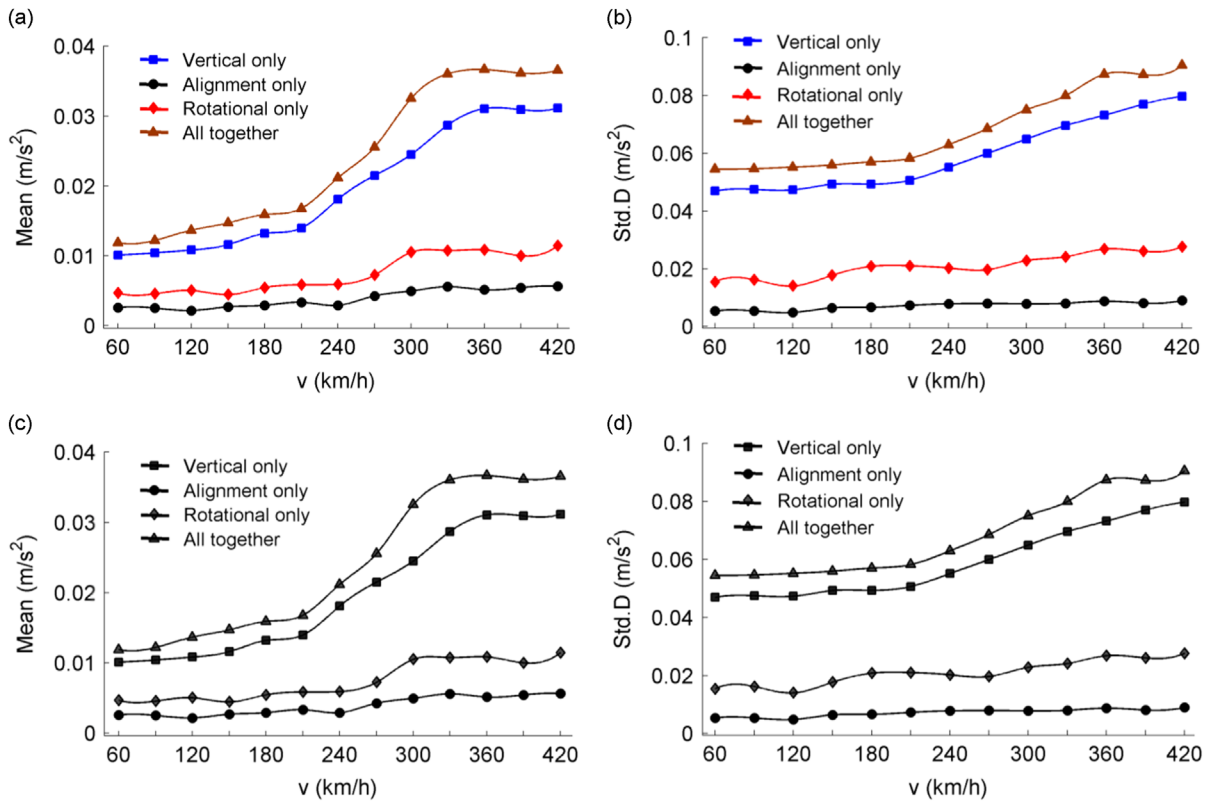


Fig. 7. Trend analysis of vertical acceleration at the gravity center of the first car-body at speeds 60–420 km/h: (a) mean value curve and (b) standard deviation curve.

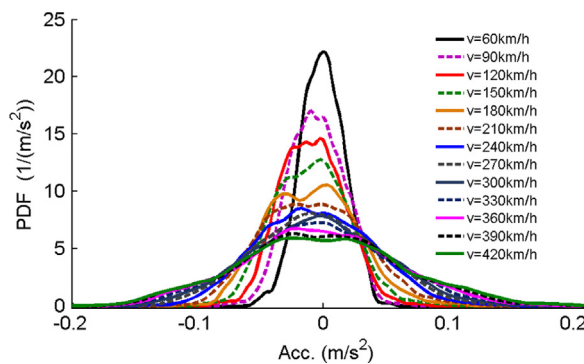


Fig. 8. Probability density function of vertical acceleration at the gravity center of the first carriage-body at the time train runs across the bridge mid-span.

3.3.1. Analysis of responses for the train

The computed maximum accelerations of vehicles in the vertical direction are shown in Figs. 6 and 7. Vertical and lateral accelerations show a similar trend: with the increase of train speed, the mean and standard deviation values of the maximum vehicle acceleration increase within certain range of speed.

The trend curves in Fig. 7 show that the acceleration with all track irregularity samples combined is clearly greater than that in other track conditions at each speed level. Nevertheless, the vertical dynamic response of the train system caused by the vertical profile track irregularity is nearly 300 percent higher than that in the other two conditions (see Fig. 7).

The probability density function of vertical acceleration of the first vehicle-body gravity center, when the train is running across the mid-span of the bridge's first-span at the speed from 60 km/h to 420 km/h, is shown in Fig. 8. The peak of probability density function of vertical vehicle acceleration is close to zero and the curvilinear shape of each curve is approximately symmetric. Furthermore, the probability distribution scope expands gradually and the peak value of each probability density decreases gradually with the increase of train speed. The results indicate that the vehicle response becomes larger when the train speed increases. This is consistent with the observations discussed in Fig. 7.

3.3.2. Dynamic analysis of bridge responses

The problem of vehicle-bridge interaction has been studied extensively, especially the dynamic characteristics of the bridge changing with the increase of train speed. However, different studies were focused on varying structures, e.g. the long-span bridge [18,31–34], prestressed concrete continuous beam bridge [35–37], prestressed concrete simple supported beam-bridge [1,16,38–42] and so on. Particularly, this paper proposed the dynamic analysis of simply supported beam bridge under different train speeds, and the computed results of bridge responses at the mid-span in vertical directions are shown in Figs. 9 and 10.

Different types of rail irregularity were adopted to study their influences on the train-bridge system vibration in this study. As shown in Figs. 9 and 10, except for the gravitational load of the vehicles, vertical profile rail irregularity is the main source of excitation that makes greater influence on the deflection and acceleration of the bridge in the vertical direction, as compared with the other types of track irregularities. Nevertheless, the mean values of the maximum bridge acceleration are almost consistent in the close-up details in Figs. 9(b) and 10(b) at the speed $v=300$ km/h.

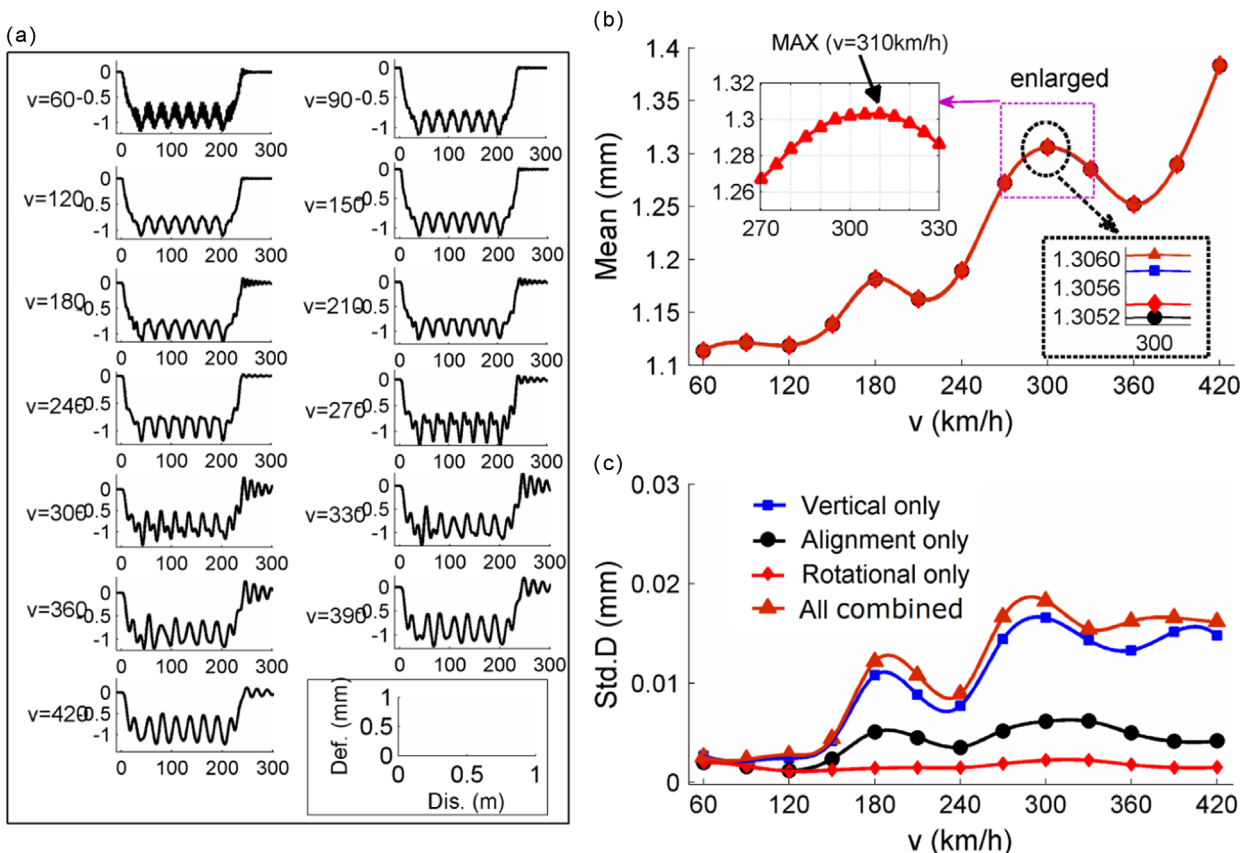


Fig. 9. Trend analysis on the vertical deflection at bridge midspan: (a) vertical deflection curve of each speed level; (b) mean value curves; and (c) standard deviation curves.

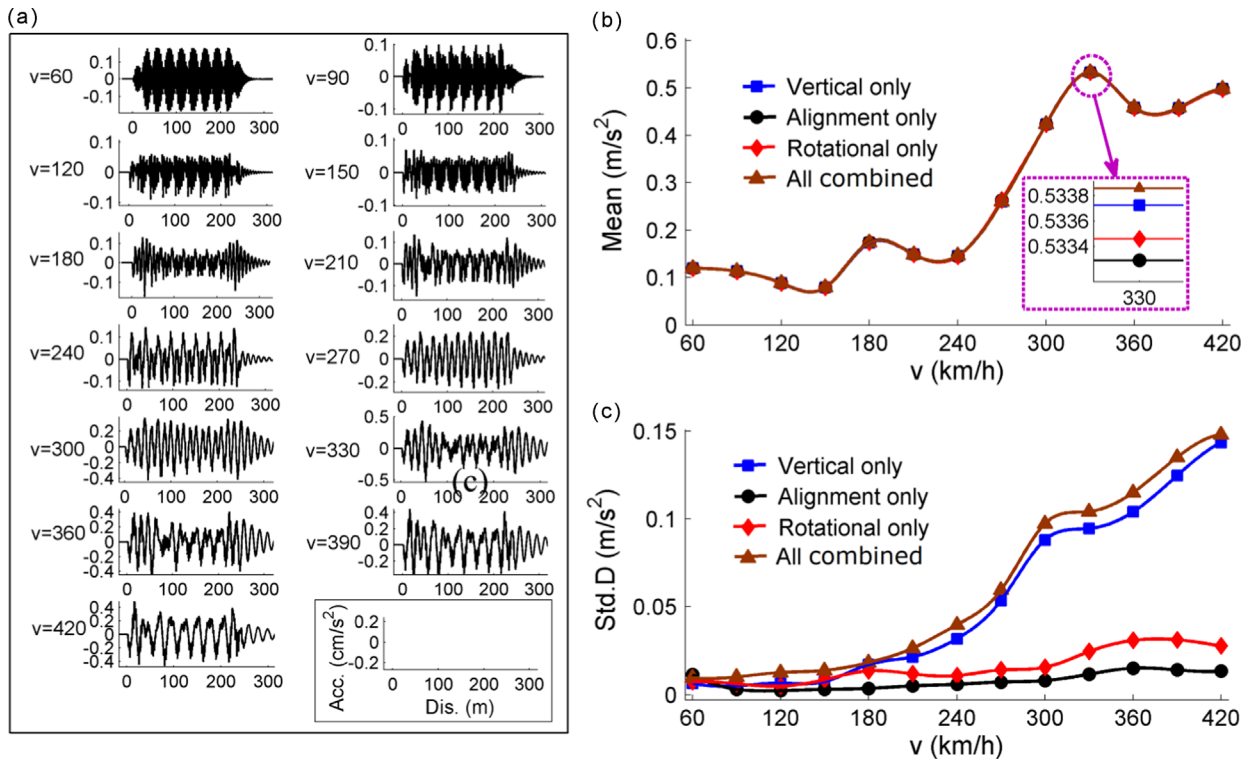


Fig. 10. Trend analysis of vertical acceleration at bridge midspan: (a) vertical acceleration curve of each speed; (b) mean value curves; and (c) standard deviation curves.

The maximum average of vertical bridge acceleration curves and the vertical bridge deflection curves, which are shown in Figs. 9 and 10, increase with increasing train speed, reach the first peak at a speed of 180 km/h and the highest peak near a speed of 300 km/h, after which the values decrease and level off at higher speed. The reason for this phenomenon may be that the forced vibration frequency of vehicle is close to the natural vibration frequency of bridge at a particular speed. That is, the forced vibration frequency of vehicle is about 4.82 Hz, which is close to the natural vibration frequency of bridge, 5.12 Hz, at a speed of 300 km/h, and the dynamic response of bridge is amplified because of resonance. To be more specific, for more detail, the mean value curve of vertical bridge deflection corresponding to the speed value ranging from 270 km/h to 330 km/h is plotted in Fig. 9(b) with a speed increment of 5 km/h. As shown in Fig. 9(b), the resonance may occur at the speed of 310 km/h. At this speed, the forced vibration frequency is close to the bridge's natural frequency. On the whole, the faster the train speed is, the greater the vertical bridge response will be, within certain range of speed.

The time-history curves in Figs. 9(a) and 10(a) at speeds from 60 km/h to 420 km/h show that the vertical bridge acceleration and deflection have many high-frequency components at lower speeds. This finding seems to be related to the forced vibration frequency of the train.

The vibration of the train-bridge system exhibits a random dynamic pattern when the vehicles travel across the bridge. This means that the maximum bridge response is considered to be random due to the random rail irregularity. Therefore, results obtained from deterministic calculations cannot accurately reveal the random vibration characteristics of the train-bridge system.

As compared to the results documented in the literature [31,38,40], the trends of dynamic characteristic curves of bridge at the mid-span section corresponding to different train speeds, either shown as curves in Figs. 9 and 10 or reported previously in the literatures, are considered to be essentially consistent. It can be seen that the mean value curves for dynamic bridge responses in Figs. 9(b) and 10(b) increase with increasing train speed within a certain speed range. Nevertheless, there also exist some small differences among individual results because the bridge parameters and vehicle parameters used in this study are different from those found in previous studies. In addition to the mean value curves, the trend of standard deviation curves for dynamic responses is also important as it reflects the random distribution of maximum responses. As shown in Fig. 9(c), the standard deviation curves of vertical bridge deflection increase with increasing train speed, and reach the first peak at a speed of 180 km/h and the greatest peak near a speed of 300 km/h. This means the maximum bridge response at the peaks is distributed over a wider range due to the resonance.

Furthermore, as compared the mean value curves and standard deviation curves in Figs. 9 and 10, the results show that the mean curves almost overlap with each other, whereas the standard deviation curves distinct significantly from each other as influenced by four different types of track irregularity. Without considering working condition of the three track

irregularities combined (all combined), the influence of vertical profile track irregularity (vertical only) on the vertical bridge response at the mid-span section is the greatest while the influence of the other two, i.e., cross-level track irregularity (alignment only) and track alignment irregularity (rotational only), significantly diminished. Therefore, in comparison with deterministic analysis approaches, the random vibration theory as PDEM may contribute to revealing the mechanisms of random vibration of the coupled train–bridge system.

4. Conclusions

A 3D coupled train–bridge random vibration system is established using PDEM and executed in the MATLAB[®] platform. The outputs include the time–history distribution of probability density evolution information, average value curves and standard deviation curves of the responses, and some discussions are made. Some conclusions are listed as follows:

- (1) Stochastic harmonic function (SHF) and number theory method (NTM) are applicable and reliable methods for generating the random rail irregularity samples. Apart from the vehicle loading, vertical profile track irregularity is the main influencing factor causing the vertical random vibration of the train–bridge system.
- (2) As compared to the MCM, the PDEM seems to be more efficient for the same accuracy level in the vibration calculation of train–bridge interaction, with an improvement of 1–2 orders of magnitude.
- (3) The responses of the train–bridge system increases with increasing train speed within a certain speed range, and the speed of 330 km/h seems to be a detrimental one for this particular system.

Acknowledgments

This study was supported by the National High Technology Research and Development Program of China (863 Program; Grant number 2009AA11Z101), the National Natural Science Foundation of China (Grant numbers 51278496, 51578549, and U1434204), and the Ministry of Science and Technology Development Projects of Railways (Grant numbers 2012G013-B and 2013G003-A-3).

References

- [1] N. Zhang, H. Xia, W.W. Guo, Vehicle–bridge interaction analysis under high-speed trains, *Journal of Sound and Vibration* 309 (2008) 407–425.
- [2] Y.B. Yang, D.J. Yau, S.Y. Wu, *Vehicle–Bridge Interaction Dynamics: With Applications to High-speed Rail*, World Scientific Pub Co Inc, Singapore, 2004.
- [3] L. Fryba, *Dynamic of Railway Bridges*, Thomas Telford, London, 1996.
- [4] H. Xia, G. De Roeck, H.R. Zhang, N. Zhang, Dynamic analysis of train–bridge system and its application in steel girder reinforcement, *Computers and Structures* 79 (2001) 1851–1860.
- [5] W.M. Zhai, K.Y. Wang, C.B. Cai, Fundamentals of vehicle–track coupled dynamics, *Vehicle System Dynamics* 47 (2009) 1349–1376.
- [6] L. Fryba, Non-stationary response of a beam to a moving random force, *Journal of Sound and Vibration* 46 (1976) 323–338.
- [7] R. Iwankiewicz, P. Sniady, Vibration of a beam under a random stream of moving forces, *Journal of Structure Mechanics* 12 (1984) 13–26.
- [8] P. Sniady, S. Biemat, R. Sieniawska, Vibration of the beam due to a load moving with stochastic velocity, *Probabilistic Engineering Mechanics* 16 (2001) 53–59.
- [9] K.H. Chu, V.K. Garg, C.L. Dhar, Railway–bridge impact: simplified train and bridge model, *Journal of the Structural Division, ASCE* 105 (1979) 1823–1844.
- [10] H.S. Zibdeh, H.S. Juma, Dynamic response of a rotating beam subjected to a random moving load, *Journal of Sound and Vibration* 223 (1999) 741–758.
- [11] F. Lu, J.H. Lin, D. Kennedy, F.W. Williams, An algorithm to study non-stationary random vibrations of vehicle–bridge systems, *Computers and Structures* 87 (2009) 177–185.
- [12] Q.Y. Zeng, X.R. Guo, *Train–Bridge Time-Variant System Analysis Theory and Application*, China Railway Press, Beijing, 1999.
- [13] W.M. Zhai, Z.X. He, X.L. Song, Prediction of high-speed train induced ground vibration based on train–track–ground system model, *Earthquake Engineering and Engineering Vibration* 9 (2010) 545–554.
- [14] X.Y. Liu, W.M. Zhai, Analysis of vertical dynamic wheel/rail interaction caused by polygonal wheels on high-speed trains, *Wear* 314 (2014) 282–290.
- [15] W.M. Zhai, C.B. Cai, Train/track/bridge dynamic interactions: simulation and applications, *Vehicle System Dynamics* 37S (2002) 653–665.
- [16] P. Antolin, N. Zhang, J.M. Goicolea, H. Xia, M.A. Astiz, J. Oliva, Consideration of nonlinear wheel–rail contact forces for dynamic vehicle–bridge interaction in high-speed railways, *Journal of Sound and Vibration* 332 (2013) 1231–1251.
- [17] N. Zhang, H. Xia, W.W. Guo, G. De Roeck, A vehicle–bridge linear interaction model and its validation, *International Journal of Structural Stability and Dynamics* 10 (2010) 335–361.
- [18] H. Xia, W.W. Guo, N. Zhang, G.J. Sun, Dynamic analysis of a train–bridge system under wind action, *Computers and Structures* 86 (2008) 1845–1855.
- [19] E. Kardas-Cinal, Spectral distribution of derailment coefficient in Non-Linear model of railway vehicle–track system with random track irregularities, *Journal of Computational and Nonlinear Dynamics* 8 (2013) 1–9.
- [20] Z.C. Zhang, J.H. Lin, Y.H. Zhang, W.P. Howson, F.W. Williams, Non-stationary random vibration analysis of three-dimensional train–bridge systems, *Vehicle System Dynamics* 48 (2010) 457–480.
- [21] J. Li, J.B. Chen, W.L. Sun, Y.B. Peng, Advances of the probability density evolution method for nonlinear stochastic systems, *Probabilistic Engineering Mechanics* 28 (2012) 132–142.
- [22] J. Li, J.B. Chen, *Stochastic Dynamics of Structures*, John Wiley & Sons (Asia) Pte Ltd, 2009.
- [23] J. Li, J.B. Chen, The principle of preservation of probability and the generalized density evolution equation, *Structural Safety* 30 (2008) 65–77.
- [24] Z.W. Yu, J.F. Mao, A. Et, The stochastic analysis of theTrack–bridge vertical coupled vibration with random train parameters, *Journal of the China Railway Society* 37 (2015) 97–104.
- [25] J.B. Chen, W.L. Sun, J. Li, J. Xu, Stochastic harmonic function representation of stochastic processes, *Journal of Applied Mechanics-Transactions of the ASME* 80 (2013) 1–11.
- [26] J.B. Chen, J. Li, Optimal determination of frequencies in the spectral representation of stochastic processes, *Computational Mechanics* 51 (2013) 791–806.

- [27] H. Xia, N. Zhang, *Dynamic Interaction of Vehicles and Structure*, 2nd edition, Science press, Beijing, China, 2005.
- [28] W.L. Sun, J.B. Chen, J. Li, Stochastic harmonic functions of second kind for spectral representations, *Journal of Tongji University (Natural Science)* (2011) 1413–1419.
- [29] K.T. Fang, D. Lin, Uniform design in computer and physical experiments, *Grammar of Technology Development* (2008) 105–125.
- [30] Y.D. Zhou, K.T. Fang, An efficient method for constructing uniform designs with large size, *Computational Statistics* 28 (2013) 1319–1331.
- [31] Y. Li, S. Dong, Y. Bao, K. Chen, S. Qiang, Impact coefficient analysis of long-span railway cable-stayed bridge based on coupled vehicle–bridge vibration, *Shock and Vibration* (2015) 1–9.
- [32] J.D. Yau, Dynamic response analysis of suspended beams subjected to moving vehicles and multiple support excitations, *Journal of Sound and Vibration* 325 (2009) 907–922.
- [33] D. Bruno, F. Greco, P. Lonetti, Dynamic impact analysis of long span cable-stayed bridges under moving loads, *Engineering Structures* 30 (2008) 1160–1177.
- [34] H. Xia, Y.L. Xu, T. Chan, Dynamic interaction of long suspension bridges with running trains, *Journal of Sound and Vibration* 237 (2000) 263–280.
- [35] Z. Zeng, Y. Zhao, W. Xu, Z. Yu, L. Chen, P. Lou, Random vibration analysis of train–bridge under track irregularities and traveling seismic waves using train–slab track–bridge interaction model, *Journal of Sound and Vibration* 342 (2015) 22–43.
- [36] Y.M. Cao, H. Xia, Z.H. Li, A semi-analytical/FEM model for predicting ground vibrations induced by high-speed train through continuous girder bridge, *Journal of Mechanical Science and Technology* 26 (2012) 2485–2496.
- [37] X.Q. Zhu, S.S. Law, Precise time–step integration for the dynamic response of a continuous beam under moving loads, *Journal of Sound and Vibration* 240 (2001) 962–970.
- [38] K. Youcef, T. Sabiha, D. El Mostafa, D. Ali, M. Bachir, Dynamic analysis of train–bridge system and riding comfort of trains with rail irregularities, *Journal of Mechanical Science and Technology* 27 (2013) 951–962.
- [39] Y.B. Yang, J.D. Yau, An iterative interacting method for dynamic analysis of the Maglev train–guideway/foundation–soil system, *Engineering Structures* 33 (2011) 1013–1024.
- [40] Y.S. Wu, Y.B. Yang, Steady-state response and riding comfort of trains moving over a series of simply supported bridges, *Engineering Structures* 25 (2003) 251–265.
- [41] W.W. Guo, H. Xia, G. De Roeck, K. Liu, Integral model for train–track–bridge interaction on the Sesia viaduct: dynamic simulation and critical assessment, *Computers and Structures* 112 (2012) 205–216.
- [42] Z. Zeng, X. He, Y. Zhao, Z. Yu, L. Chen, W. Xu, P. Lou, Random vibration analysis of train–slab track–bridge coupling system under earthquakes, *Structural Engineering and Mechanics* 54 (2015) 1017–1044.